

Modeling of Viscoelastic Electromechanical Behavior in a Soft Dielectric Elastomer Actuator

Guo-Ying Gu, *Member, IEEE*, Ujjaval Gupta, Jian Zhu, Li-Min Zhu, *Member, IEEE*,
and Xiangyang Zhu, *Member, IEEE*

Abstract—Soft dielectric elastomer actuators (DEAs) exhibit interesting muscle-like behavior for the development of soft robots. However, it is challenging to model these soft actuators due to their material nonlinearity, nonlinear electromechanical coupling, and time-dependent viscoelastic behavior. Most recent studies on DEAs focus on issues of mechanics, physics, and material science, while much less importance is given to quantitative characterization of DEAs. In this paper, we present a detailed experimental investigation probing the voltage-induced electromechanical response of a soft DEA that is subjected to cyclic loading and propose a general constitutive modeling approach to characterize the time-dependent response, based on the principles of nonequilibrium thermodynamics. In this paper, some of the key observations are found as follows: 1) Creep exhibits the drift phenomenon, and is dominant during the first three cycles. The creep decreases over time and becomes less dominant after the first few cycles; 2) a significant amount of hysteresis is observed during all cycles and it becomes repeatable after the first few cycles; 3) the peak of the displacement is shifted from the peak of the voltage signal and occurs after it. To account for these viscoelastic phenomena, a constitutive model is developed by employing several dissipative nonequilibrium mechanisms. The quantitative comparisons of the experimental and simulation results demonstrate the effectiveness of the developed model. This modeling approach can be useful for control of a viscoelastic DEA and paves the way to emerging applications of soft robots.

Index Terms—Creep, dielectric elastomer actuator (DEA), hysteresis, soft robotics, viscoelastic electromechanical modeling.

I. INTRODUCTION

As the frontier of robotics is moving into new applications, such as unstructured constrained spaces or human-centered environments where safety and adaptability to the uncertainties are fundamental requirements, soft actuators with their inherent flexibility and tendency to conform to the external environment become important to the development of soft robots [1], [2].

In recent years, several soft actuators based on pneumatic or fluidic technology [3]–[5] and shape memory alloys [6], [7] have been de-

veloped for soft robots that have attracted significant attention in the robotics society. However, it is usually difficult to achieve a precise and fast control of the compressed air or temperature. Alternatively, dielectric elastomer actuators (DEAs) are one kind of electrically driven soft actuators [8], [9], which can deform in response to voltage, and exhibit interesting attributes including large deformation, fast response, and inherent flexibility. DEAs can be fabricated in various shapes or sizes to perform different functions [10]–[12]. Recently, DEAs have been employed to develop a jellyfish robot [13], a hexapod robot [14], an annelid robot [15], and an artificial muscle to mimic the movement of human jaw [16]. The reader may refer to [10] and [17]–[19] for detailed information on applications of DEAs.

A DEA has a multilayered structure, consisting of a thin membrane of elastomer sandwiched between two compliant electrodes. When subjected to voltage, the elastomer experiences the Maxwell stress and responds by contracting in thickness while expanding in area simultaneously [10], [19]. Although the working principle of the DEA looks simple, the behavior of the DEA can be complex due to material nonlinearity and nonlinear electromechanical coupling behavior such as the electrical breakdown and electromechanical instability [20], [21]. Besides, the DEA exhibits viscoelasticity and its behavior is strongly time dependent.

Many previous works have been performed for modeling the DEAs [22]–[34]. Some models were employed for qualitative (rather than quantitative) interpretation of mechanics and physical phenomena, for example, electromechanical phase transition in a laterally clamped membrane [26]. Some models were simplified, using a linear viscoelasticity model [24], [25], ignoring inhomogeneous deformation [27] or linearizing the system [28], which could affect their accuracy especially when the deformation is large. Some models were developed without detailed experimental verifications [29].

It is expected for a DEA made of viscoelastic elastomer such as the VHB 4905/4910 to show time-dependent nonlinearities upon cyclic loading, such as the coupled creep and hysteresis [35]–[37]. With extensive applications of DEAs to soft robots [13], [14], [16], [19], it is necessary and important to understand such viscoelastic response of the DEAs with a quantitative model. To address this challenge, a general modeling framework is proposed in this paper to quantitatively characterize the nonlinear time-dependent electromechanical response of DEAs subjected to cyclic loading voltage. For this purpose, real-time experiments are conducted on a custom-built DEA under different protocols of cyclic loading voltage. Then, the comprehensive experimental phenomena of voltage-induced deformation including the viscoelastic creep and hysteresis are investigated. Finally, a constitutive model based on the principles of nonequilibrium thermodynamics is developed to interpret these phenomena. Results predicted by the developed model are then compared to the experimental data, which quantifies its effectiveness with appreciable accuracy.

This paper is novel in that a dissipative thermodynamic model is employed, which not only qualitatively but also quantitatively interpret

Manuscript received January 16, 2017; accepted May 3, 2017. Date of publication May 29, 2017; date of current version October 2, 2017. This paper was recommended for publication by Associate Editor P. Fraitse and Editor P. Dupont upon evaluation of the reviewers' comments. This work was supported in part by the National Natural Science Foundation of China under Grant 51622506 and Grant 51620105002, in part by the Science and Technology Commission of Shanghai Municipality under Grant 16JC1401000, and in part by MOE Tier 1, Singapore, under Grant R-265-000-497-112 and Grant R-265-000-558-112. (*Guo-Ying Gu and Ujjaval Gupta contributed equally to this work.*) (*Corresponding author: Guo-Ying Gu.*)

G.-Y. Gu, L.-M. Zhu, and X. Zhu are with the State Key Laboratory of Mechanical System and Vibration, School of Mechanical Engineering, Shanghai Jiao Tong University, Shanghai 200240, China (e-mail: guguying@sjtu.edu.cn; zhulm@sjtu.edu.cn; mexyzy@sjtu.edu.cn).

U. Gupta and J. Zhu are with the Department of Mechanical Engineering, National University of Singapore, Singapore, 117575 (e-mail: ujjaval.gupta@nus.edu.sg; mpezhu@nus.edu.sg).

Color versions of one or more of the figures in this paper are available online at <http://ieeexplore.ieee.org>.

Digital Object Identifier 10.1109/TRO.2017.2706285

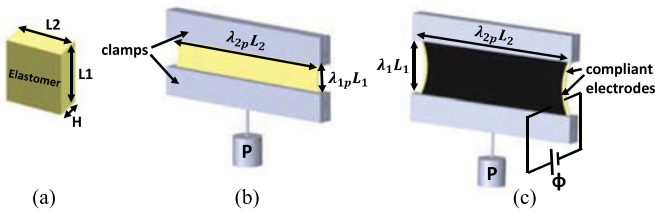


Fig. 1. Schematic of the DEA. (a) Reference state. (b) Prestretched state. (c) Current state. In the prestretched and the current state, $\lambda_2 = \text{constant} = \lambda_{2p}$.

viscoelastic electromechanical behavior including creep, hysteresis, and voltage-induced deformation. The results show that the soft actuators electromechanical behavior can be accurately predicted, which may pave the way for precise control of soft actuators/robots.

The rest of this paper is organized as follows. The experimental setup is introduced in Section II. Section III presents the experimental results followed by a discussion on the viscoelastic phenomena observed in experiments. In Section IV, the constitutive model is detailed and Section V shows the theoretical and experimental comparisons for different voltage signals. Finally, the conclusion of this study is drawn in Section VI.

II. SYSTEM DESCRIPTION

A. Dielectric Elastomer Actuator

In this paper, a clamped soft DEA is fabricated as shown in Fig. 1. This laterally clamped actuator is easy to fabricate, and is able to provide linear actuation with 1 DOF. The laterally clamped actuator has recently been employed to mimic facial muscles to achieve jaw movement [16]. It is known that the material viscoelasticity can significantly affect the electromechanical behavior of the DEA such as phase transitions to wrinkling, and these effects can be qualitatively interpreted by a viscoelastic model [26]. However, how to accurately predict the deformation of the actuator remains an interesting open question. Therefore, this clamped soft DEA is adopted in this paper for experimental analysis and constitutive modeling.

The working principle of the developed DEA can be described as follows.

- 1) In the reference state, the size of the elastomer is $L_1 \times L_2 \times H$, where length $L_1 = 20$ mm, width $L_2 = 70$ mm, and thickness $H = 1$ mm. The dielectric elastomer membrane made of 3M VHB4910 is prestretched by $\lambda_{2p} = 2$ and fixed to rigid clamps at two ends. A constant mechanical force P is applied by a dead load that vertically prestretches the membrane by $\lambda_{1p} = 1.5$.
- 2) In the prestretched state, the length of the membrane is $\lambda_{1p} L_1 = 30$ mm and the width is $\lambda_{2p} L_2 = 140$ mm. The elastomer is coated with carbon grease on both sides of the prestretched membrane as compliant electrodes.
- 3) In the current state, the membrane is subjected to voltage ϕ and the length of the elastomer changes to $\lambda_1 L_1$ with width $\lambda_{2p} L_2$.

It is well known that the DEA may suffer failure, instability, or loss of tension [21], [26], [38] with high voltages. In this paper, we mainly focus on investigating the behavior of DEAs when subjected to cyclic loading voltages. The maximum voltage is therefore kept low to prevent any loss of tension, instability or dielectric breakdown.

B. Experimental Setup

The experimental setup with the fabricated DEA is shown in Fig. 2. For the phenomena observation, tens of samples of DEAs were made

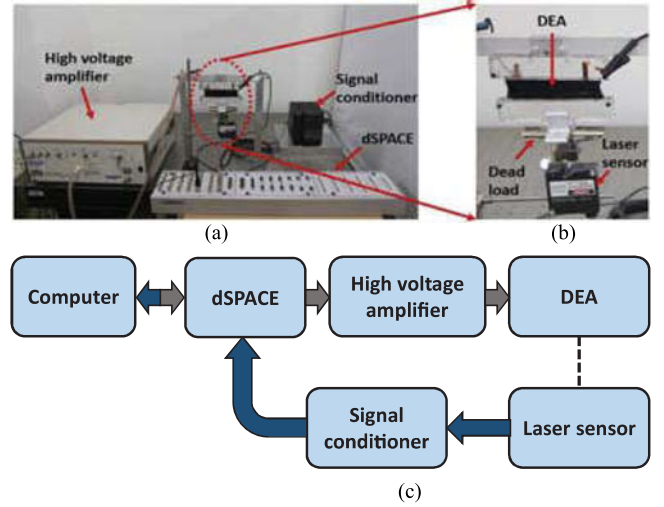


Fig. 2. (a) Experimental setup, (b) DEA, and (c) block diagram of the setup.

in the experiments. A dSPACE-DS1103 control board equipped with 16-bit analog-to-digital converters and 16-bit digital-to-analog converters (DACs) is employed to generate different patterns of cyclic loading voltage. The DACs output the analog control voltage, which is then amplified with a fixed gain of 1000 by the high-voltage amplifier (10/40 A, Trek, Inc.). The real-time displacement of the DEA is measured by a laser displacement sensor (LK-G5000, Keyence) with a stroke of 6 mm and resolution of 10 nm. The sampling time of the dSPACE board is set to be 1 ms. Furthermore, the MATLAB/Simulink software is used to implement the algorithms, which are directly downloaded to the dSPACE-DS1103 control board via the ControlDesk interface for conducting experiments in real time. The tests are conducted at room temperature, hence the temperature-dependent behaviors of the DEA can be ignored.

III. EXPERIMENTAL RESULTS

A. Voltage Loading Patterns

To investigate the response of the designed DEA, four kinds of periodic voltage patterns with different loading histories are employed. As an illustration, Fig. 3(a) shows one period of voltage pattern 1 (VP1) with only one maximum peak, (b) shows one period of voltage pattern 2 (VP2) with three increasing local maximum peaks, (c) shows one period of voltage pattern 3 (VP3) with three decreasing local minimum peaks, and (d) shows one period of voltage pattern 4 (VP4) with both increasing and decreasing local maximum peaks. The different voltage patterns are significant to understand the amplitude dependent characteristics of the viscoelastic behavior in the DEA during extension and contraction, respectively, which will be discussed in detail later.

B. Experimental Observations

In this section, we will first investigate the complex viscoelastic behavior in the DEA when the simple VP1 is applied to drive the DEA. The experimental results are analyzed to study the different viscoelastic behavior such as creep and hysteresis. A constitutive model with several dissipative nonequilibrium mechanisms is proposed in Section IV to quantitatively capture the experimental data. In the following section, the experimental responses to VP2, VP3, and VP4 are quantitatively

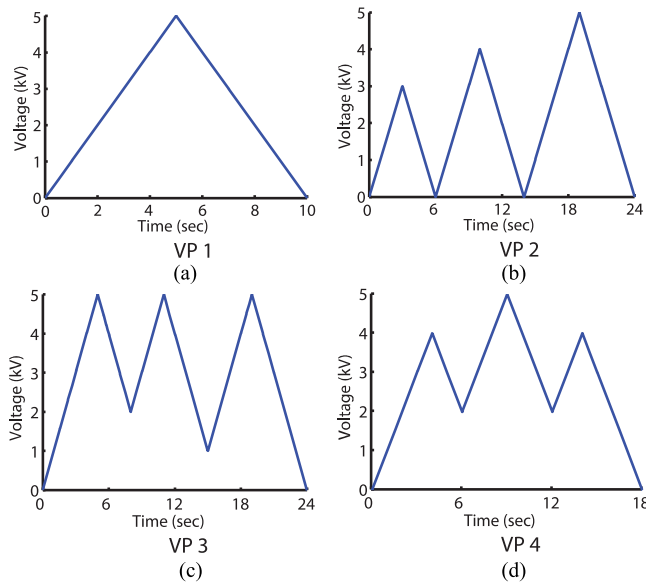


Fig. 3. Four different triangular voltage patterns applied to the DEA. (a) Voltage Pattern 1, VP1 with only one maximum peak. (b) VP2 with three increasing local maximum peaks. (c) VP3 with three decreasing local minimum peaks. (d) VP4 with both increasing and decreasing local maximum peaks.

compared with the model prediction to demonstrate the effectiveness of the model.

Fig. 4 shows the experimental results with VP1, where (a) shows the input voltage with 12 cycles and (b) shows the experimental response of the DEA. It can be seen that the response exhibits strong nonlinear phenomena coupled with viscoelasticity. The major experimental observations are outlined below.

- 1) The first phenomenon observed is the drift of the displacement with time as shown in Fig. 4(b), which is generally called the viscoelastic creep. Significant amount of creep is observed in the first three cycles [see Fig. 4(b) and (d)] and it decreases over time and becomes less dominant after the first few cycles [see Fig. 4(b) and (e)].
- 2) The second phenomenon is significant amount of hysteresis. When subjected to cyclic voltage, the electromechanical response of the DEA is different during unloading as compared to loading. After the first three cycles, the loading and unloading paths of each hysteresis loop become similar in shape. It is worthy of mentioning that the maximum displacement, which is reached at the maximal applied voltage, also increases with the number of cycles as shown in Fig. 4(c), which can be interpreted as the effects of the viscoelastic creep. Fig. 4(e) shows the response after the first three cycles when the creep is removed. It can be seen that the hysteresis loop becomes repeatable.
- 3) Another interesting phenomenon is related to the shift of the peak of the displacement from the peak of the voltage signal. As can be seen from Fig. 4(d), the peak of the displacement is observed during the unloading part and appears after the maximum applied voltage.

The above observations demonstrate that the electromechanical response of the DEA when subjected to cyclic voltage is a nonlinear and nonequilibrium process and the energy is dissipated during the loading-unloading cycle. To quantitatively account for these nonlinear phenomena in DEAs with an effective and accurate model is one of the important objectives of this study.

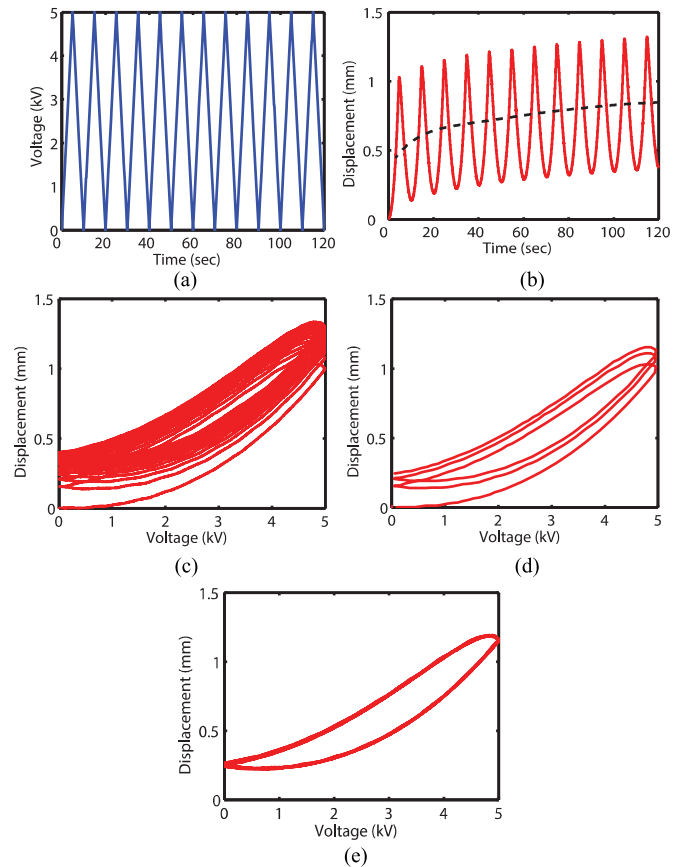


Fig. 4. Experimental response of the DEA subject to twelve cycles of VP1. (a) Voltage as a function of time. (b) Experimentally recorded displacement as a function of time. (c) Displacement as a function of voltage for the first three cycles. (d) Displacement as a function of voltage for the last nine cycles. (e) Displacement as a function of voltage for the last nine cycles, when the displacement due to creep is ignored (i.e., the actuator is assumed to return to the same displacement when voltage vanishes in each cycle). The actuator exhibits repeatable hysteresis.

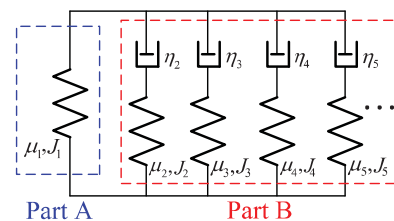


Fig. 5. Rheological representation of the two-part constitutive model. The model consists of an elastic spring in parallel with several viscoelastic units, each of which consists of an elastic spring in series with a viscous dashpot.

IV. CONSTITUTIVE MODELING

The experimental data in the previous section clearly show that upon cyclic loading voltage, the DEA exhibits complicated time-dependent nonlinear response. In this paper, a two-part constitutive model on the basis of nonequilibrium thermodynamics is developed to incorporate these time-dependent response.

Fig. 5 shows a rheological representation of the proposed two-part constitutive model. The first part *A* with a nonlinear spring describes the equilibrium state and the second part *B* with a set of nonlinear springs and linear dashpots captures the nonlinear time-dependent deviation from the equilibrium state. The number of the nonlinear springs and

Algorithm: Model Evolution

Input: Input voltage signal, material and geometrical parameters
Output: Prediction of time-dependent electromechanical response of the actuator

- 1 **begin**
- 2 Input mechanic parameters of the spring J_i, μ_i (where $i=1,2,3,\dots,n$) and the relaxation time of the dashpots T_j (where $j=1,2,3,\dots,n-1$)
- 3 Input dielectric permittivity ε of the material
- 4 Input geometrical parameters $\lambda_{1p}, \lambda_{2p}, L_1, L_2, H$
- 5 Input voltage signal $\phi(t)$
- 6 Initialize the variables $\lambda_k, \lambda_2, \xi_{k1}, \xi_{k2}$ where $k=2,3,4,\dots,n$
- 7 Call the **ode45** function **visco** for the specified time interval t
- 8 Get the voltage value ϕ_i at time instant t_i
- 9 Calculate $d\lambda_k/dt, d\xi_{k1}/dt, d\xi_{k2}/dt$ for given ϕ_i using system of equations in 15
- 10 Integrate to find $\lambda_k(t), \xi_{k1}(t)$ and $\xi_{k2}(t)$
- 11 **end**
- 12 **end**

Fig. 6. Algorithm for solving (15).

linear dashpots is generally determined based on the experimental data and predicted accuracy of the developed model. The constitutive model can be developed as follows.

In the current state, the DEA is subject to voltage ϕ through the thickness, charge Q of opposite sign accumulates on two electrodes, and the membrane experiences force P_1 and P_2 in plane parallel to the length and width, respectively. As a result, the size of the DEA membrane changes to length l_1 , width l_2 , and thickness h . The stretches of the membrane can, therefore, be defined as $\lambda_1 = l_1/L_1, \lambda_2 = l_2/L_2$, and $\lambda_3 = h/H$. The membrane is assumed to be incompressible, i.e., $\lambda_1 \lambda_2 \lambda_3 = 1$. The true stresses in the membrane can be defined as $\sigma_1 = P_1/(l_2 h), \sigma_2 = P_2/(l_1 h)$, the true electric field is $E = \phi/h$, and the true electric displacement is $D = Q/(l_1 l_2)$. Based on the theory of nonequilibrium thermodynamics [39], the increase in the free energy δG should be less than or equal to the work done by the mechanical forces and the electrical voltage

$$\delta G \leq P_1 \delta l_1 + P_2 \delta l_2 + \phi \delta Q \quad (1)$$

where Q can be expressed as $Q = \varepsilon \frac{\phi}{H} L_1 L_2 (\lambda_1 \lambda_2)^2$ by considering the membrane of the DEA as a stretchable capacitor.

The free energy density can be obtained by dividing free energy of the elastomer with the volume of the membrane, i.e., $W = G/(L_1 L_2 H)$, therefore

$$\delta W \leq \frac{\sigma_1}{\lambda_1} \delta \lambda_1 + \frac{\sigma_2}{\lambda_2} \delta \lambda_2 + 2\varepsilon \left(\frac{\phi}{H} \right)^2 (\lambda_1 \lambda_2^2 \delta \lambda_1 + \lambda_1^2 \lambda_2 \delta \lambda_2). \quad (2)$$

For the ideal dielectric elastomer, the Helmholtz free energy density W can be assumed to be a function of the set of independent variables given by

$$W(\lambda_1, \lambda_2, D, \xi_{21}, \xi_{22}, \dots) = W_s(\lambda_1, \lambda_2, \xi_{21}, \xi_{22}, \dots) + \frac{D^2}{2\varepsilon} \quad (3)$$

where $\xi_{21}, \xi_{22}, \dots$ represent the set of internal variables characterizing the time-dependent behavior of the dielectric elastomer; ε is the permittivity of the dielectric elastomer, satisfying $\varepsilon = D/E$; W_s is associated with the stretching of the elastomer; $\frac{D^2}{2\varepsilon}$ is associated with the polarization of the elastomer.

As shown in Fig. 5, the stretches of the spring in part A are given by λ_1 and λ_2 , which are same as the stretches of the DEA. The stretches of

the springs in part B are given by λ_{i1}^e and λ_{i2}^e , and the stretches of the dashpot are given by ξ_{i1} and ξ_{i2} , where $i(= 2, 3, 4, \dots, n)$ represents the number of the spring-dashpot units. Since all the parallel units have the same net stretches, the stretches can be related by the following equations $\lambda_1 = \lambda_{i1}^e \xi_{i1}, \lambda_2 = \lambda_{i2}^e \xi_{i2}$ [26].

To describe the free energy density associated with the stretching of the DEA, the Gent model [19] is employed in this paper. Therefore, the free energy density corresponding to stretching is given by the sum of stretching energy density of all the springs as

$$\begin{aligned} W_s(\lambda_1, \lambda_2, \xi_{21}, \xi_{22}, \xi_{31}, \xi_{32}, \xi_{41}, \xi_{42}, \dots, \xi_{n1}, \xi_{n2}) \\ = -\frac{\mu_1 J_1}{2} \log \left(1 - \frac{\lambda_1^2 + \lambda_2^2 + \lambda_1^{-2} \lambda_2^{-2} - 3}{J_1} \right) \\ - \sum_{i=2}^n \frac{\mu_i J_i}{2} \log \left(1 - \frac{\lambda_1^2 \xi_{i1}^{-2} + \lambda_2^2 \xi_{i2}^{-2} + \lambda_1^{-2} \lambda_2^{-2} \xi_{i1}^2 \xi_{i2}^2 - 3}{J_i} \right) \end{aligned} \quad (4)$$

where μ_1 and μ_i represent the shear strain modulus of the springs, and J_1 and J_i are constants relating to the maximum stretch limit of the respective spring. It should be mentioned that other material models such as Neo-Hookean and Mooney-Rivlin models [19] can also be used to describe the free energy density relating the stress and strain because the strain in this paper is restricted to be small to avoid dielectric breakdown. Without loss of generality, we prefer to use a Gent model because it can demonstrate the strain-stiffening effect of an elastomer.

By combining (2)–(4), we can obtain

$$\begin{aligned} \sigma_1 + \varepsilon E^2 = \mu_1 \frac{\lambda_1^2 - \lambda_1^{-2} \lambda_2^{-2}}{1 - (\lambda_1^2 + \lambda_2^2 + \lambda_1^{-2} \lambda_2^{-2} - 3)/J_1} \\ + \sum_{i=2}^n \mu_i \frac{\lambda_1^2 \xi_{i1}^{-2} - \lambda_1^{-2} \lambda_2^{-2} \xi_{i1}^2 \xi_{i2}^2}{1 - (\lambda_1^2 \xi_{i1}^{-2} + \lambda_2^2 \xi_{i2}^{-2} + \lambda_1^{-2} \lambda_2^{-2} \xi_{i1}^2 \xi_{i2}^2 - 3)/J_i} \end{aligned} \quad (5)$$

$$\begin{aligned} \sigma_2 + \varepsilon E^2 = \mu_1 \frac{\lambda_2^2 - \lambda_1^{-2} \lambda_2^{-2}}{1 - (\lambda_1^2 + \lambda_2^2 + \lambda_1^{-2} \lambda_2^{-2} - 3)/J_1} \\ + \sum_{i=2}^n \mu_i \frac{\lambda_2^2 \xi_{i2}^{-2} - \lambda_1^{-2} \lambda_2^{-2} \xi_{i1}^2 \xi_{i2}^2}{1 - (\lambda_1^2 \xi_{i1}^{-2} + \lambda_2^2 \xi_{i2}^{-2} + \lambda_1^{-2} \lambda_2^{-2} \xi_{i1}^2 \xi_{i2}^2 - 3)/J_i} \end{aligned} \quad (6)$$

Assuming the dashpot to be a Newtonian fluid with viscosity η_i , the strain rate of the dashpot is given by $\xi_{i1}^{-1} d\xi_{i1}/dt$ and $\xi_{i2}^{-1} d\xi_{i2}/dt$, which can be expressed as

$$\begin{aligned} \frac{1}{\xi_{i1}} \frac{d\xi_{i1}}{dt} = \frac{1}{3\eta_i} \left(\frac{\mu_i (\lambda_1^2 \xi_{i1}^{-2} - \xi_{i1}^2 \xi_{i2}^2 \lambda_1^{-2} \lambda_2^{-2})}{1 - (\lambda_1^2 \xi_{i1}^{-2} + \lambda_2^2 \xi_{i2}^{-2} + \xi_{i1}^2 \xi_{i2}^2 \lambda_1^{-2} \lambda_2^{-2} - 3)/J_i} \right. \\ \left. - \frac{\mu_i (\lambda_2^2 \xi_{i2}^{-2} - \xi_{i1}^2 \xi_{i2}^2 \lambda_1^{-2} \lambda_2^{-2})/2}{1 - (\lambda_1^2 \xi_{i1}^{-2} + \lambda_2^2 \xi_{i2}^{-2} + \xi_{i1}^2 \xi_{i2}^2 \lambda_1^{-2} \lambda_2^{-2} - 3)/J_i} \right) \quad (7) \\ \frac{1}{\xi_{i2}} \frac{d\xi_{i2}}{dt} = \frac{1}{3\eta_i} \left(\frac{\mu_i (\lambda_2^2 \xi_{i2}^{-2} - \xi_{i1}^2 \xi_{i2}^2 \lambda_1^{-2} \lambda_2^{-2})}{1 - (\lambda_1^2 \xi_{i1}^{-2} + \lambda_2^2 \xi_{i2}^{-2} + \xi_{i1}^2 \xi_{i2}^2 \lambda_1^{-2} \lambda_2^{-2} - 3)/J_i} \right. \\ \left. - \frac{\mu_i (\lambda_1^2 \xi_{i1}^{-2} - \xi_{i1}^2 \xi_{i2}^2 \lambda_1^{-2} \lambda_2^{-2})/2}{1 - (\lambda_1^2 \xi_{i1}^{-2} + \lambda_2^2 \xi_{i2}^{-2} + \xi_{i1}^2 \xi_{i2}^2 \lambda_1^{-2} \lambda_2^{-2} - 3)/J_i} \right). \quad (8) \end{aligned}$$

It can be proved that the developed model satisfies the thermodynamic inequality (2) when $\eta_i > 0$. The viscoelastic relaxation time can be related to the viscosity of the dashpot and the shear modulus of the spring as

$$T_{i-1} = \eta_i / \mu_i, \quad i = 2, 3, 4, \dots, n. \quad (9)$$

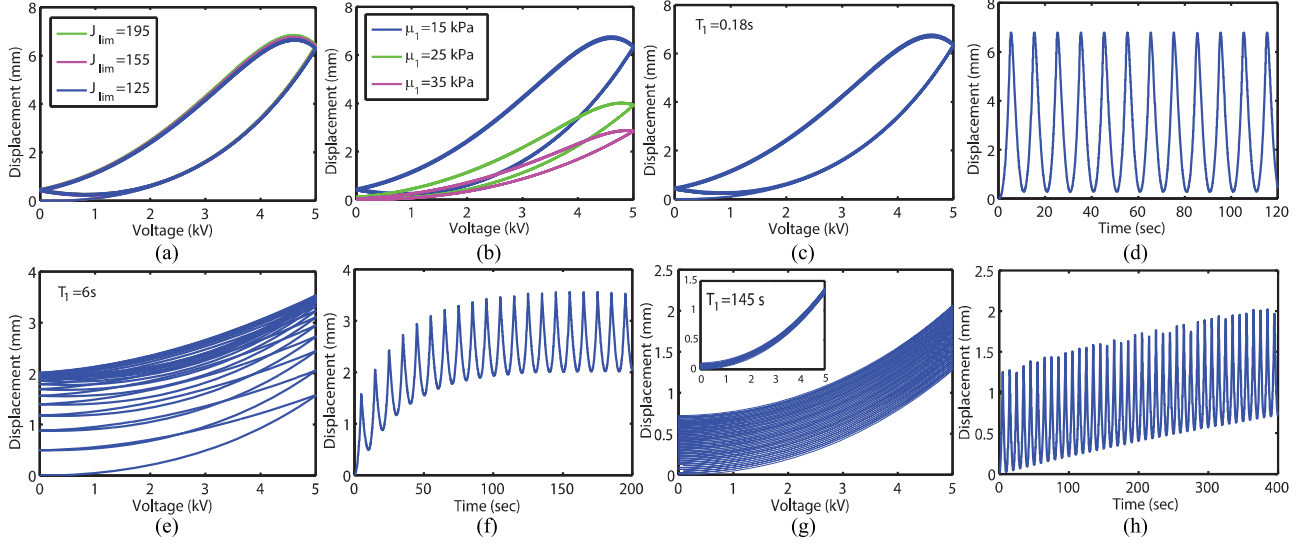


Fig. 7. Influence of material parameters on the simulation response of Model I (with single spring-dashpot element) to several cycles of VP1. (a) Displacement versus voltage for different stretch limits ($J_1 = J_2 = J_{lim}$). Shear modulus and relaxation time are kept constant ($\mu_1 = 15$ kPa, $\mu_2 = 50$ kPa, $T_1 = 0.18$ s). (b) Displacement versus voltage for different shear modulus. Stretch limit and relaxation time are kept constant ($J_1 = J_2 = 155$, $\mu_2 = 50$ kPa, $T_1 = 0.18$ s). (c)–(h) Displacement versus voltage and displacement versus time, respectively, for different relaxation time. Stretch limit and shear modulus are kept constant ($J_1 = J_2 = 155$, $\mu_1 = 15$ kPa, $\mu_2 = 50$ kPa), where relaxation time $T_1 = 0.18$ s in (c) and (d), relaxation time $T_1 = 6$ s in (e) and (f), and relaxation time $T_1 = 145$ s in (g) and (h). First five cycles of model response are shown in inset of (g).

At time $t = 0$, we assume that $\phi = 0$ and the dashpots have been given enough time to be fully relaxed. Thus, the initial conditions are given by $\lambda_1 = \lambda_{1p}$, $\lambda_2 = \lambda_{2p}$, $\xi_{i1} = \lambda_{1p}$, and $\xi_{i2} = \lambda_{2p}$. Substituting the initial conditions into (5), we get the stress σ_1 in vertical direction as

$$\sigma_1 = \mu_1 \frac{\lambda_{1p}^2 - \lambda_{1p}^{-2} \lambda_{2p}^{-2}}{1 - (\lambda_{1p}^2 + \lambda_{2p}^2 + \lambda_{1p}^{-2} \lambda_{2p}^{-2} - 3)/J_1}. \quad (10)$$

By substituting $\sigma_1 = P_1/(l_2 h)$ ($l_2 = \lambda_{2p} L_2$ and $h = \lambda_3 H$), the load P_1 in the vertical direction can be expressed as

$$P_1 = \mu_1 L_2 H \frac{\lambda_{1p} - \lambda_{1p}^{-3} \lambda_{2p}^{-2}}{1 - (\lambda_{1p}^2 + \lambda_{2p}^2 + \lambda_{1p}^{-2} \lambda_{2p}^{-2} - 3)/J_1}. \quad (11)$$

Furthermore, if we substitute $\sigma_1 = P_1/(l_2 h)$ and $E = \phi/h$ directly into (5), P_1 can be represented as

$$P_1 = f(\phi, \lambda_1, \lambda_2, \xi_{21}, \xi_{22}, \dots, \xi_{n1}, \xi_{n2}). \quad (12)$$

Considering the fact that P_1 given by (11) is constant, therefore $dP_1/dt = 0$. Differentiating (12) with respect to time, we get

$$\frac{dP_1}{dt} = \frac{\partial P_1}{\partial \phi} \frac{d\phi}{dt} + \frac{\partial P_1}{\partial \lambda_1} \frac{d\lambda_1}{dt} + \frac{\partial P_1}{\partial \lambda_2} \frac{d\lambda_2}{dt} + \sum_{i=2}^n \left(\frac{\partial P_1}{\partial \xi_{i1}} \frac{d\xi_{i1}}{dt} + \frac{\partial P_1}{\partial \xi_{i2}} \frac{d\xi_{i2}}{dt} \right) = 0. \quad (13)$$

According to the clamped membrane fabrication of the DEA, the stretch $\lambda_2 = \lambda_{2p}$ is fixed, which results in $d\lambda_2/dt = 0$. Therefore, (13) can be re-expressed as

$$\frac{d\lambda_1}{dt} = \left(-\frac{\partial P_1}{\partial \phi} \frac{d\phi}{dt} + \sum_{i=2}^n \left(-\frac{\partial P_1}{\partial \xi_{i1}} \frac{d\xi_{i1}}{dt} - \frac{\partial P_1}{\partial \xi_{i2}} \frac{d\xi_{i2}}{dt} \right) \right) / \frac{\partial P_1}{\partial \lambda_1}. \quad (14)$$

Combining (14) with (7) and (8), a set of differential equations can be obtained in (15), shown at the bottom of this page. The voltage is then applied to the system. For the prescribed cyclic voltage $\phi(t)$, (15) can be used for evolution of $\lambda_1(t)$, $\lambda_2(t)$, $\xi_{i1}(t)$, and $\xi_{i2}(t)$. The algorithm for solving the equations in (15) is briefly listed in Fig. 6.

$$\begin{bmatrix} d\lambda_1/dt \\ d\xi_{21}/dt \\ d\xi_{22}/dt \\ \vdots \\ d\xi_{n1}/dt \\ d\xi_{n2}/dt \end{bmatrix} = \begin{bmatrix} \left(-\frac{\partial P_1}{\partial \phi} \frac{d\phi}{dt} + \sum_{i=2}^n \left(-\frac{\partial P_1}{\partial \xi_{i1}} \frac{d\xi_{i1}}{dt} - \frac{\partial P_1}{\partial \xi_{i2}} \frac{d\xi_{i2}}{dt} \right) \right) / \frac{\partial P_1}{\partial \lambda_1} \\ \frac{\xi_{21}}{3\eta_2} \left(\frac{\mu_2 (\lambda_1^2 \xi_{21}^{-2} - \xi_{21}^2 \xi_{22}^2 \lambda_1^{-2} \lambda_2^{-2})}{1 - (\lambda_1^2 \xi_{21}^{-2} + \lambda_2^2 \xi_{22}^{-2} + \xi_{21}^2 \xi_{22}^2 \lambda_1^{-2} \lambda_2^{-2} - 3)/J_2} - \frac{\mu_2 (\lambda_2^2 \xi_{22}^{-2} - \xi_{21}^2 \xi_{22}^2 \lambda_1^{-2} \lambda_2^{-2})/2}{1 - (\lambda_1^2 \xi_{21}^{-2} + \lambda_2^2 \xi_{22}^{-2} + \xi_{21}^2 \xi_{22}^2 \lambda_1^{-2} \lambda_2^{-2} - 3)/J_2} \right) \\ \frac{\xi_{22}}{3\eta_2} \left(\frac{\mu_2 (\lambda_2^2 \xi_{22}^{-2} - \xi_{21}^2 \xi_{22}^2 \lambda_1^{-2} \lambda_2^{-2})}{1 - (\lambda_1^2 \xi_{21}^{-2} + \lambda_2^2 \xi_{22}^{-2} + \xi_{21}^2 \xi_{22}^2 \lambda_1^{-2} \lambda_2^{-2} - 3)/J_2} - \frac{\mu_2 (\lambda_1^2 \xi_{21}^{-2} - \xi_{21}^2 \xi_{22}^2 \lambda_1^{-2} \lambda_2^{-2})/2}{1 - (\lambda_1^2 \xi_{21}^{-2} + \lambda_2^2 \xi_{22}^{-2} + \xi_{21}^2 \xi_{22}^2 \lambda_1^{-2} \lambda_2^{-2} - 3)/J_2} \right) \\ \vdots \\ \frac{\xi_{n1}}{3\eta_n} \left(\frac{\mu_n (\lambda_1^2 \xi_{n1}^{-2} - \xi_{n1}^2 \xi_{n2}^2 \lambda_1^{-2} \lambda_2^{-2})}{1 - (\lambda_1^2 \xi_{n1}^{-2} + \lambda_2^2 \xi_{n2}^{-2} + \xi_{n1}^2 \xi_{n2}^2 \lambda_1^{-2} \lambda_2^{-2} - 3)/J_n} - \frac{\mu_n (\lambda_2^2 \xi_{n2}^{-2} - \xi_{n1}^2 \xi_{n2}^2 \lambda_1^{-2} \lambda_2^{-2})/2}{1 - (\lambda_1^2 \xi_{n1}^{-2} + \lambda_2^2 \xi_{n2}^{-2} + \xi_{n1}^2 \xi_{n2}^2 \lambda_1^{-2} \lambda_2^{-2} - 3)/J_n} \right) \\ \frac{\xi_{n2}}{3\eta_n} \left(\frac{\mu_n (\lambda_2^2 \xi_{n2}^{-2} - \xi_{n1}^2 \xi_{n2}^2 \lambda_1^{-2} \lambda_2^{-2})}{1 - (\lambda_1^2 \xi_{n1}^{-2} + \lambda_2^2 \xi_{n2}^{-2} + \xi_{n1}^2 \xi_{n2}^2 \lambda_1^{-2} \lambda_2^{-2} - 3)/J_n} - \frac{\mu_n (\lambda_1^2 \xi_{n1}^{-2} - \xi_{n1}^2 \xi_{n2}^2 \lambda_1^{-2} \lambda_2^{-2})/2}{1 - (\lambda_1^2 \xi_{n1}^{-2} + \lambda_2^2 \xi_{n2}^{-2} + \xi_{n1}^2 \xi_{n2}^2 \lambda_1^{-2} \lambda_2^{-2} - 3)/J_n} \right) \end{bmatrix} \quad (15)$$

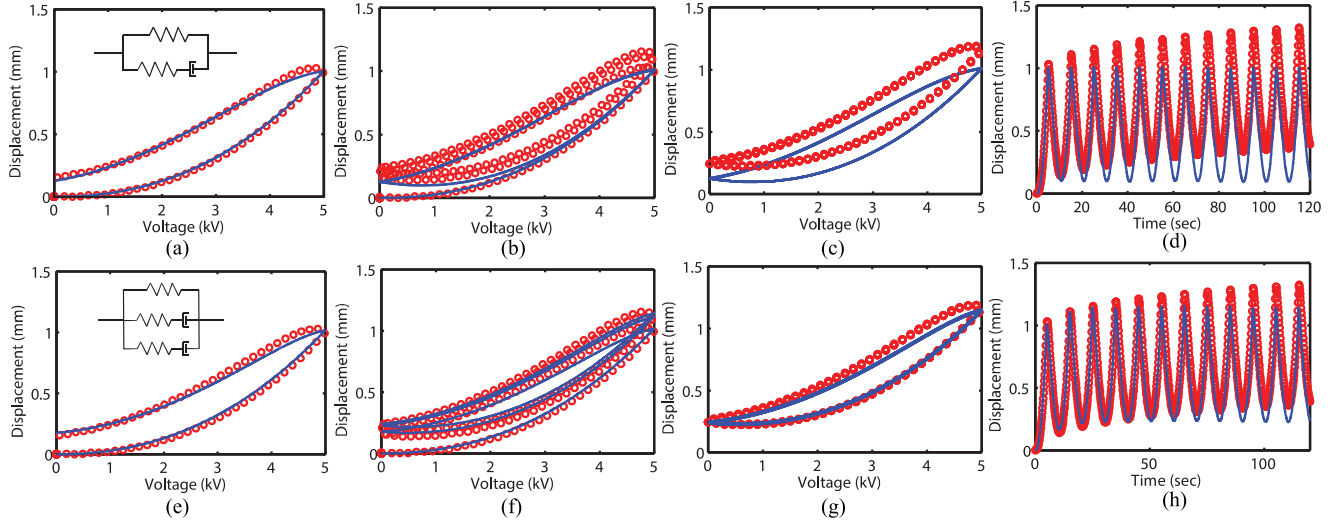


Fig. 8. Simulation results of the DEA subjected to 12 cycles of VP1, for two models, Model I [see (a)–(d)] and Model II [see (e)–(h)]. The blue curves represent the model prediction, while the red circles represent the experiments. (a)–(d) Model I, which combines an elastic spring and a viscoelastic element. (e)–(h) Model II, which combines an elastic spring and two viscoelastic elements. (a) and (e) Displacement as a function of voltage for the first cycle. (b) and (f) Displacement as a function of voltage for the first three cycles. (c) and (g) Displacement as a function of voltage for the last nine cycles, with the creep effect ignored. (d) and (h) Displacement as a function of time.

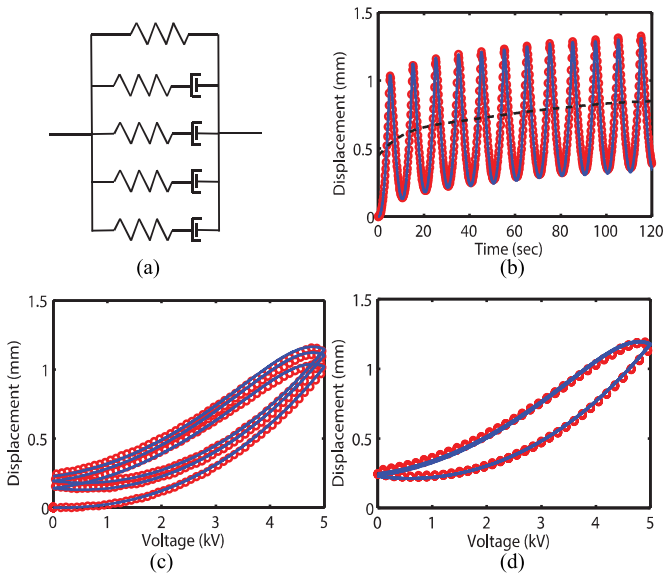


Fig. 9. (a) Comparison between the experimental and simulation results of the DEA subjected to 12 cycles of VP1 for the developed model, which consists of an elastic spring in parallel with four viscoelastic units. In (b)–(d), the blue curves represent the model prediction, while the red circles represent the experiments. (b) Displacement as a function of time. (c) Displacement as a function of voltage for the first three cycles. (d) Displacement as a function of voltage for the last nine cycles, with the creep effect ignored.

V. RESULTS AND DISCUSSIONS

In this section, the comparative experimental results are presented to verify the effectiveness of the developed model.

A. Influence of the Model Parameters

First, we try to investigate the influence of shear modulus, relaxation time, and stretch limit on the time-dependent response of the soft DEA. A single spring-dashpot unit as shown in part B of the two-part

constitutive model (see Fig. 5), referring to as Model I, is adopted to simulate the effect of different material parameters.

Fig. 7(a) shows the model prediction with different stretch limits when several cycles of VP1 [as shown in Fig. 3(a)] are applied. It can be seen that changing the stretch limit does not have much influence on the model response. This may be because the material undergoes deformation smaller than the limiting stretch. Fig. 7(b) shows the model prediction with different shear modulus. It is evident that the response of the model shows larger deformation when the shear modulus is small. This is attributed to the fact that low shear modulus represents soft material and under the same stress a softer material has a larger deformation. Fig. 7(c)–(h) shows the influence of relaxation time. Fig. 7(c) and (d) shows the results with a small relaxation time ($T_1 = 0.18$ s). When the viscoelastic relaxation time is very small, the dashpot achieves equilibrium very quickly as can be seen in Fig. 7(d). The response of the model is dominated by a large hysteresis loop with negligible creep and the response becomes repeatable after the first cycle, as shown in Fig. 7(c). Fig. 7(e) and (f) shows the results with a moderate relaxation time of $T_1 = 6$ s. It can be seen that as the relaxation time increases, the time taken to achieve equilibrium also increases. Furthermore, it can be seen from Fig. 7(e) that the hysteresis loop becomes smaller with the increase of the relaxation time. Moreover, the response of the material predicted by the model shows significant creep in the first few cycles and the response of the material becomes repeatable after several cycles, as shown in Fig. 7(e). It can be seen from Fig. 7(f) that the creep becomes negligible after several cycles. Fig. 7(g) and (h) shows the model response with higher relaxation time of $T_1 = 145$ s. It can be seen that the response of the material shows creep over longer period of time and the hysteresis becomes nearly negligible.

Based on the above results, we will take the following steps to fit the material parameters for verifying the effectiveness of the developed models. At the first step, we tune the shear modulus to fit the hysteresis loop in the first cycle. The graph in Fig. 7(b) shows how the shear modulus affects the hysteresis loop, especially for the first cycle. At the second step, we tune the relaxation times of the dashpots to fit the creep deformations and the hysteresis loops af-

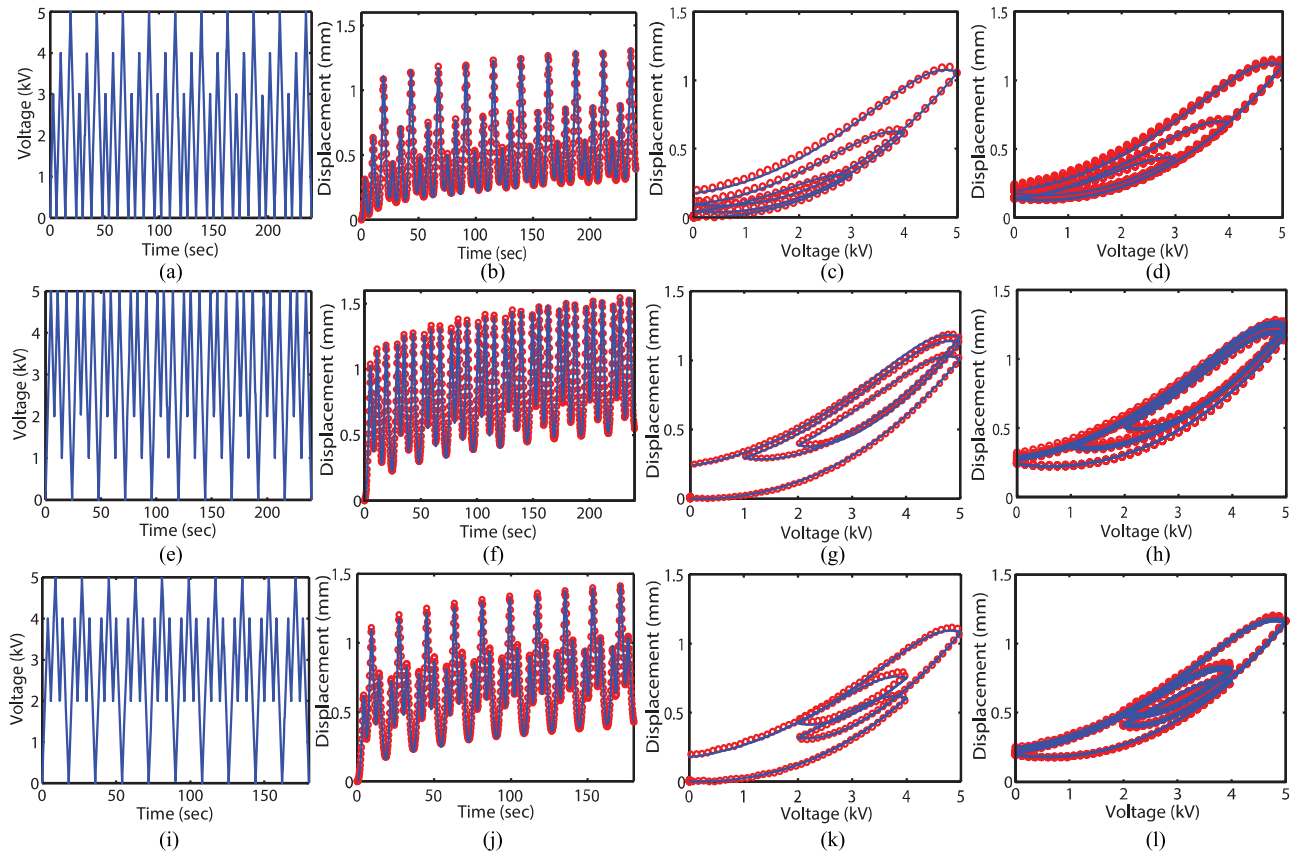


Fig. 10. Comparison between the experimental and simulation results of the DEA subjected to ten cycles of voltage pattern. Progression of plots from left to right: (a) Voltage signal applied to the DEA. In (b)–(d), the blue curves represent the model prediction, while the red circles represent the experiments. (b) Displacement as a function of time. (c) Displacement as a function of voltage for the first three cycles. (d) Displacement as a function of voltage for the last nine cycles, with the creep effect ignored. Top to bottom: VP2, VP3, VP4.

ter the second cycle. Fig. 7(c), (e), and (g) shows the effects of relaxation times on the creep deformations and the hysteresis loops. We then repeat the first and second steps until the differences between the simulations and the experiments are within acceptable range.

B. Model Comparison

We next try to understand the effect of spring-dashpot units on the viscoelastic response by employing two different models (Model I and Model II). Model I is with single spring-dashpot unit [see inset Fig. 8(a)], and Model II is with two spring-dashpot units [see inset Fig. 8(e)].

Fig. 8(a)–(d) shows the predicted results with Model I. The material parameters used in the simulation are: $J_1 = J_2 = 155$, $\mu_1 = 78$ kPa, $\mu_2 = 65$ kPa, and $T_1 = 0.85$ s. Fig. 8(a) compares the experimental response for the first cycle of the triangular voltage in red circle with the theoretical results in blue curve. It can be seen that the hysteresis within the first cycle of the experimental response can be fit very well with Model I. Fig. 8(b) shows the output for first three cycles. As discussed in Section III-B, significant creep is observed in the first three cycles [see Fig. 4(d)], but this effect cannot be predicted with Model I. Furthermore, Fig. 8(d) shows that the creep cannot be predicted well with Model I. According to the experimental observation [see Fig. 4(e)], the hysteresis becomes repeatable after the first few cycles. Fig. 8(c) shows that the repeatable nature of the hysteresis loop can be predicted with Model I. However, the loop is

shifted downward, which may be due to the simplistic nature of the model.

Fig. 8(e)–(h) shows the predicted results with Model II. The material parameters used in the simulation are $J_1 = J_2 = J_3 = 155$, $\mu_1 = 62$ kPa, $\mu_2 = 40$ kPa, $\mu_3 = 30$ kPa, $T_1 = 0.5$ s, and $T_2 = 5$ s. Fig. 8(e) shows a good agreement between the model prediction and the experimental response for the hysteresis within the first cycle. Comparing the result in Fig. 8(b) to that of (f), we can see that by adding an extra spring-dashpot unit in the model, the creep effect can be predicted better, which can also be verified by (h). Similarly, Fig. 8(g) shows that the repeatable nature of the hysteresis loops can be predicted, which are in good agreement with the experiment. Comparing the results of Model II [see Fig. 8(e)–(h)] with those of Model I [see Fig. 8(a)–(d)], it can be concluded that adding more parallel units of spring-dashpot helps in predicting the viscoelastic effects more accurately.

C. Model Validation

Considering the experimental observations and comparison with the simulation results, four spring-dashpot units are adopted in the developed model to account for the coupled creep and hysteresis due to the viscoelasticity. The values of the different material parameters are given as $J_1 = J_2 = J_3 = J_4 = J_5 = 155$, shear modulus are given by $\mu_1 = 15$ kPa, $\mu_2 = 150$ kPa, $\mu_3 = 20$ kPa, $\mu_4 = 25$ kPa, $\mu_5 = 12$ kPa, and relaxation time by $T_1 = 0.18$ s, $T_2 = 6$ s, and $T_3 = 145$ s, $T_4 = 550$ s. Fig. 9 shows good agreement between the model prediction and the experimental response with the predicted

root-mean-squared error less than 3%. It should be noted that further increase of the numbers (more than 4) of spring-dashpot units leads to little improvement in accuracy, but makes the computation more costly. Without loss of generality, we use four spring-dashpot units for the following verification.

To further verify the developed model, three other voltage patterns VP2-4 with different amplitude histories [see Fig. 3(b)–(d)] are employed to drive the DEA. We should mention that all the material parameters in the model are kept same as tuned for VP 1. Fig. 10 shows the quantitative comparison of the model prediction and the experimental response of the DEA for different voltage patterns. It can be seen that the experimental observations are precisely predicted by the developed model, which well verifies the effectiveness of the model. It can be observed that depending upon the loading histories with different amplitudes, the hysteresis of the DEA shows the memory effects with both the major loop and the minor loop. Without considering the physics nature of the hysteresis behavior, it is interesting to see similar phenomena in the hysteresis loops with both the wiping-out and congruency properties as usually discussed in other smart material actuators such as the piezoelectric and shape memory alloys actuators [40]–[42]. The wiping-out property refers to the nonlocal memoryless behavior, which means that the hysteresis output depends upon not only the current input but also the previous dominant input extrema. In other words, only the alternating series of the dominant input extrema are stored by the hysteresis loops, and all other input extrema are wiping out, as can be seen in Fig. 10(d) and (h). The congruency property means that the two minor hysteresis loops corresponding to the same input range are congruent. From Fig. 10(i), it can be observed that if the lower minor hysteresis loop in the loading path is shifted up along the vertical direction without any rotation, it can approximately overlap the higher loop in the unloading path. We should mention that these two properties are essential for the well-known mathematical hysteresis models such as the Preisach model and Prandtl–Ishlinskii model [40]–[42]. These analogue phenomena may provide an alternative modeling method for the future analysis of the hysteresis behavior in the DEA.

VI. CONCLUSION

In this paper, we investigate the electromechanical response of a clamped planar DEA when subjected to cyclic voltage. Voltage of four different patterns was applied and the DEA was found to exhibit strong nonlinear phenomena coupled with viscoelasticity, such as creep, hysteresis, and other viscoelastic effects. A nonlinear viscoelastic model is developed that can accurately predict the electromechanical response of the DEA subjected to cyclic voltage of different patterns. This paper leads to a better understanding of the nonlinear electromechanical phenomena coupled with viscoelasticity in DEAs. It is expected that precise prediction of the electromechanical response of DEAs will lead to their successful control, which may be useful in extensive emerging applications of soft robots.

REFERENCES

- [1] D. Rus and M. T. Tolley, "Design, fabrication and control of soft robots," *Nature*, vol. 521, no. 7553, pp. 467–475, 2015.
- [2] A. Albu-Schäffer *et al.*, "Soft robotics," *IEEE Robot. Autom. Mag.*, vol. 15, no. 3, pp. 20–30, Sep. 2008.
- [3] J. Bishop-Moser and S. Kota, "Design and modeling of generalized fiber-reinforced pneumatic soft actuators," *IEEE Trans. Robot.*, vol. 31, no. 3, pp. 536–545, Jun. 2015.
- [4] P. Polygerinos *et al.*, "Modeling of soft fiber-reinforced bending actuators," *IEEE Trans. Robot.*, vol. 31, no. 3, pp. 778–789, Jun. 2015.
- [5] A. D. Marchese and D. Rus, "Design, kinematics, and control of a soft spatial fluidic elastomer manipulator," *Int. J. Robot. Res.*, vol. 35, pp. 840–869, 2016.
- [6] H. T. Lin, G. G. Leisk, and B. Trimmer, "Goqbot: A caterpillar-inspired soft-bodied rolling robot," *Bioinspiration Biomimetics*, vol. 6, no. 2, 2011, Art. no. 026007.
- [7] B. Mazzolai, L. Margheri, M. Cianchetti, P. Dario, and C. Laschi, "Soft-robotic arm inspired by the octopus: II. From artificial requirements to innovative technological solutions," *Bioinspiration Biomimetics*, vol. 7, no. 2, 2012, Art. no. 025005.
- [8] F. Carpi, S. Bauer, and D. De Rossi, "Stretching dielectric elastomer performance," *Science*, vol. 330, no. 6012, pp. 1759–1761, 2010.
- [9] I. M. Koo, K. Jung, J. C. Koo, J. D. Nam, Y. K. Lee, and H. R. Choi, "Development of soft-actuator-based wearable tactile display," *IEEE Trans. Robot.*, vol. 24, no. 3, pp. 549–558, Jun. 2008.
- [10] P. Brochu and Q. Pei, "Advances in dielectric elastomers for actuators and artificial muscles," *Macromol. Rapid Commun.*, vol. 31, no. 1, pp. 10–36, 2010.
- [11] F. Carpi, R. Kornbluh, P. Sommer-Larsen, D. De Rossi, and F. C. Alici, "Guest editorial: Introduction to the focused section on electroactive polymer mechatronics," *IEEE/ASME Trans. Mechatronics*, vol. 16, no. 1, pp. 1–7, Feb. 2011.
- [12] G. Rizzello, D. Naso, A. York, and S. Seelecke, "Modeling, identification, and control of a dielectric electro-active polymer positioning system," *IEEE Trans. Control Syst. Technol.*, vol. 23, no. 2, pp. 632–643, Mar. 2015.
- [13] H. Godaba, J. Li, Y. Wang, and J. Zhu, "A soft jellyfish robot driven by a dielectric elastomer actuator," *IEEE Robot. Autom. Lett.*, vol. 1, no. 2, pp. 624–631, Jul. 2016.
- [14] C. T. Nguyen *et al.*, "Printable monolithic hexapod robot driven by soft actuator," in *Proc. 2015 IEEE Int. Conf. Robot. Autom.*, 2015, pp. 4484–4489.
- [15] K. Jung, J. C. Koo, J. do Nam, Y. K. Lee, and H. R. Choi, "Artificial annelid robot driven by soft actuators," *Bioinspiration Biomimetics*, vol. 2, no. 2, pp. S42–S49, 2007.
- [16] Y. Wang and J. Zhu, "Artificial muscles for jaw movements," *Extreme Mech. Lett.*, vol. 6, pp. 88–95, 2016.
- [17] A. O'Halloran, F. O'Malley, and P. McHugh, "A review on dielectric elastomer actuators, technology, applications, and challenges," *J. Appl. Phys.*, vol. 104, no. 7, 2008, Art. no. 071101.
- [18] I. A. Anderson, T. A. Gisby, T. G. McKay, B. M. O'Brien, and E. P. Calius, "Multi-functional dielectric elastomer artificial muscles for soft and smart machines," *J. Appl. Phys.*, vol. 112, no. 4, 2012, Art. no. 041101.
- [19] G. Y. Gu, J. Zhu, L. M. Zhu, and X. Y. Zhu, "A survey on dielectric elastomer actuators for soft robots," *Bioinspiration Biomimetics*, vol. 12, 2017, Art. no. 011003.
- [20] J. Plante and S. Dubowsky, "Large-scale failure modes of dielectric elastomer actuators," *Int. J. Solids Struct.*, vol. 43, no. 25, pp. 7727–7751, 2006.
- [21] X. Zhao and Z. Suo, "Theory of dielectric elastomers capable of giant deformation of actuation," *Phys. Rev. Lett.*, vol. 104, no. 17, 2010, Art. no. 178302.
- [22] H. R. Choi *et al.*, "Biomimetic soft actuator: Design, modeling, control, and applications," *IEEE/ASME Trans. Mechatronics*, vol. 10, no. 5, pp. 581–593, Oct. 2005.
- [23] H. R. Choi *et al.*, "Soft actuator for robotic applications based on dielectric elastomer: quasi-static analysis," in *Proc. IEEE Int. Conf. Robot. Autom.*, 2002, vol. 3, pp. 3212–3217.
- [24] M. Wissler and E. Mazza, "Electromechanical coupling in dielectric elastomer actuators," *Sensors Actuators A, Physical*, vol. 138, no. 2, pp. 384–393, 2007.
- [25] M. Wissler and E. Mazza, "Modeling and simulation of dielectric elastomer actuators," *Smart Mater. Struct.*, vol. 14, no. 6, pp. 1396–1402, 2005.
- [26] M. Kollrosche, G. Kofod, Z. Suo, and J. Zhu, "Temporal evolution and instability in a viscoelastic dielectric elastomer," *J. Mech. Phys. Solids*, vol. 76, pp. 47–64, 2015.
- [27] G. Rizzello, M. Hodgins, D. Naso, A. York, and S. Seelecke, "Modeling of the effects of the electrical dynamics on the electromechanical response of a deep circular actuator with a mass–spring load," *Smart Mater. Struct.*, vol. 24, no. 9, 2015, Art. no. 094003.
- [28] R. Sarban, B. Lassen, and M. Willatzen, "Dynamic electromechanical modeling of dielectric elastomer actuators with metallic electrodes," *IEEE/ASME Trans. Mechatronics*, vol. 17, no. 5, pp. 960–967, Oct. 2012.

- [29] J. Sheng, H. Chen, B. Li, and Y. Wang, "Nonlinear dynamic characteristics of a dielectric elastomer membrane undergoing in-plane deformation," *Smart Mater. Struct.*, vol. 23, no. 4, 2014, Art. no. 045010.
- [30] T. Hoffstadt and J. Maas, "Analytical modeling and optimization of deap-based multilayer stack-transducers," *Smart Mater. Struct.*, vol. 24, no. 9, 2015, Art. no. 094001.
- [31] L. Liu, W. Sun, J. Sheng, L. Chang, D. Li, and H. Chen, "Effect of temperature on the electromechanical actuation of viscoelastic dielectric elastomers," *Europhys. Lett.*, vol. 112, no. 2, 2015, Art. no. 27006.
- [32] W. Kaal and S. Herold, "Electroactive polymer actuators in dynamic applications," *IEEE/ASME Trans. Mechatronics*, vol. 16, no. 1, pp. 24–32, Feb. 2011.
- [33] G. Berselli, R. Vertechy, M. Babič, and V. P. Castelli, "Dynamic modeling and experimental evaluation of a constant-force dielectric elastomer actuator," *J. Intell. Mater. Syst. Structures*, vol. 24, no. 6, pp. 779–791, 2013.
- [34] G. Y. Gu, U. Gupta, J. Zhu, L. M. Zhu, and X. Y. Zhu, "Feedforward deformation control of a dielectric elastomer actuator based on a nonlinear dynamic model," *Appl. Phys. Lett.*, vol. 107, no. 4, 2015, Art. no. 042907.
- [35] J. S. Bergström and M. C. Boyce, "Constitutive modeling of the large strain time-dependent behavior of elastomers," *J. Mech. Phys. Solids*, vol. 46, no. 5, pp. 931–954, 1998.
- [36] K. M. Schmoller and A. R. Bausch, "Similar nonlinear mechanical responses in hard and soft materials," *Nature Mater.*, vol. 12, no. 4, pp. 278–281, 2013.
- [37] K. M. Schmoller, P. Fernandez, R. C. Arevalo, D. L. Blair, and A. R. Bausch, "Cyclic hardening in bundled actin networks," *Nature Commun.*, vol. 1, 2010, Art. no. 134.
- [38] Z. Suo, X. Zhao, and W. H. Greene, "A nonlinear field theory of deformable dielectrics," *J. Mech. Phys. Solids*, vol. 56, no. 2, pp. 467–486, 2008.
- [39] Z. Suo, "Theory of dielectric elastomers," *Acta Mechanica Solida Sinica*, vol. 23, no. 6, pp. 549–578, 2010.
- [40] G. Y. Gu, L. M. Zhu, and C. Y. Su, "Modeling and compensation of asymmetric hysteresis nonlinearity for piezoceramic actuators with a modified prandtlcishlinskii model," *IEEE Trans. Ind. Electron.*, vol. 61, no. 3, pp. 1583–1595, Mar. 2014.
- [41] G. Y. Gu, L. M. Zhu, C. Y. Su, H. Ding, and S. Fatikow, "Modeling and control of piezo-actuated nanopositioning stages: A survey," *IEEE Trans. Autom. Sci. Eng.*, vol. 13, no. 1, pp. 313–332, Jan. 2016.
- [42] D. Hughes and J. T. Wen, "Preisach modeling of piezoceramic and shape memory alloy hysteresis," *Smart Mater. Struct.*, vol. 6, no. 3, pp. 287–300, 1997.